Buckling of Circular Cylindrical Shells with Different Moduli in Tension and Compression

ROBERT M. JONES*
The Aerospace Corporation, San Bernardino, Calif.

An exact solution is derived for buckling of circular cylindrical shells with different elastic moduli in tension and compression under arbitrary combinations of axial and lateral pressure. The combinations include those in which one component of pressure causes tension. Classical buckling theory, by which is implied a membrane prebuckled shape, is used for simply supported edge boundary conditions. General results in a form analogous to Batdorf's classical k-Z form are presented for several ratios of tensile to compressive elastic moduli. Differences in tensile and compressive moduli are observed to cause significant differences in the buckling loads. This situation is particularly acute when only a small tensile loading component exists in conjunction with an apparently dominant compressive loading component. For example, if a small axial tensile loading is present in a principally external pressure loading environment, a reduction of 17% in the external pressure buckling load from the zero axial load case can occur for a tensile modulus that is half the compressive modulus. The present results are important because current composite materials often have significantly different elastic moduli in tension and compression.

Nomenclature†

a_{ij} = compliances in stress-strain relations [Eq. (1)]
B_{ij} = extensional stiffnesses of a shell [Eq. (18)]
D_{ij} = bending stiffnesses of a shell [Eq. (19)]
E = Young's modulus
E_c = Young's modulus in compression (Fig. 1)
E_t = Young's modulus in tension (Fig. 1)
G_{tc} = shearing modulus [Eq. (5)]
k = Batdorf's loading parameters, k_x and k_y
k_x = axial compression loading parameter [Eq. (32)]
k_y = lateral pressure loading parameter [Eq. (45)]
k_1 = proportion of axial load [Eq. (27)]
k_2 = proportion of lateral load [Eq. (27)]
K_{ij} = function of material properties [Eq. (9)]
L = length of circular cylindrical shell (Fig. 3)
m = number of axial buckle half waves
$\delta M_x,\delta M_y,\delta M_{xy}$ = variations in moments per unit length during buckling
n = number of circumferential buckle waves
$\delta N_x,\delta N_y,\delta N_{xy}$ = variations in forces per unit length during buckling
$\bar{N}_x,\bar{N}_y$ = applied axial and circumferential forces per unit length
p = lateral pressure
P = axial load
R = shell middle surface radius (Fig. 3)
t = shell thickness (Fig. 3)
$\delta u,\delta v,\delta w$ = variations of axial, circumferential, and radial displacements during buckling from a membrane prebuckled shape
x,y,z = axial, circumferential, and radial coordinates on shell middle surface (Fig. 3)
Z = Batdorf's curvature parameter, $(L^2/Rt)(1-\nu^2)^{1/2}$
Z_{tc} = curvature parameter for shells with different moduli in tension and compression [Eq. (33)]
$\epsilon_x,\epsilon_y,\gamma_{xy}$ = axial, circumferential, and shear strains
$\delta\epsilon_x,\delta\epsilon_y,\delta\gamma_{xy}$ = variations in ϵ_x, ϵ_y, and γ_{xy} during buckling
ν = Poisson's ratio
ν_c = Poisson's ratio in compression
ν_t = Poisson's ratio in tension
$\sigma_x,\sigma_y,\tau_{xy}$ = axial, circumferential, and shear stresses
$\delta\sigma_x,\delta\sigma_y,\delta\tau_{xy}$ = variations in σ_x, σ_y, and τ_{xy} during buckling
$\delta\chi_1,\delta\chi_2,\delta\chi_3$ = variations in curvatures during buckling

Introduction

CURRENT composite materials, whether fiber-reinforced or granular, typically have different elastic moduli in tension and compression. This characteristic behavior is shown schematically in the stress-strain curve of Fig. 1. Some pseudoisotropic composites (i.e., layered composites that have essentially the same stiffness in all directions) involving fiberglass and boron have tensile moduli as low as 60% of the compressive moduli.[1] Orthotropic composites such as SCOTCHPLY fiberglass have compressive moduli 20% lower than the tensile moduli for unidirectional layers.[2] For SCOTCHPLY layups of six layers in one direction and five in the perpendicular direction, the compressive moduli are about 10% lower than the tensile moduli.[2] Granular composites such as ZTA graphite have tensile moduli as much as 20% lower than the compressive moduli.[3] Many other materials have different tensile and compressive moduli; which modulus is higher depends, in part, on the relation between fiber or granule stiffness and matrix stiffness. This relation, in turn, influences whether or not the fibers or granules tend to contact as well as whether the individual fibers buckle.

Actual stress-strain behavior is probably not as simple as shown in Fig. 1. Rather, a nonlinear transition region may exist between the tensile and compressive linear portions of the stress-strain curve.[4] The measurement of strains near zero stress is difficult to perform accurately, but the stress-strain behavior might be as shown in Fig. 2 where replacement of the actual behavior by the bilinear Ambartsumyan model[5] is offered as a simplification of the obviously nonlinear behavior. Moreover, for most materials, there is

Presented at the Sixth U.S. National Congress of Applied Mechanics, Harvard University, Cambridge, Mass., June 15–19, 1970; received December 29, 1969; revision received July 20, 1970.

* Member of the Technical Staff, Theoretical Mechanics Section. Presently Associate Professor of Solid Mechanics, SMU Institute of Technology, Dallas, Texas. Associate Fellow AIAA.

† A comma indicates partial differentiation with respect to the subscript following the comma. The prefix δ denotes the variation during buckling of the symbol that follows.

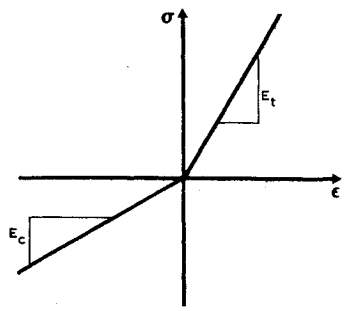

Fig. 1 Stress-strain curve for a material with different moduli in tension and compression.

inadequate mechanical property data on which to base the more complex model. One possible disadvantage of the Ambartsumyan model is that a discontinuity in slope (modulus) occurs at the origin of the stress-strain curve (see Figs. 1 and 2). The effect of the slope discontinuity is discussed in the body of the paper.

Ambartsumyan and Khachatryan discuss the basic elasticity equations and some solutions for stress analysis of shells and bodies of revolution made of materials with different moduli in tension and compression by use of the Ambartsumyan model.[5–8]‡ However, to the author's knowledge, no analysis is available to study the buckling characteristics of shells made of such materials. Usually the compressive modulus is thought of as being the governing factor in buckling problems. This reasoning is correct for buckling of uniaxial configurations such as columns or rings. However, for buckling of biaxial configurations such as plates or shells, the modulus transverse to the principal load affects the buckling load. Obviously, then, should tension occur in the transverse direction, the tensile modulus affects the buckling load.

The objective of this paper is to derive an analysis for buckling of circular cylindrical shells (see Fig. 3) that have different elastic moduli in tension and compression. The Ambartsumyan model for biaxial stress-strain behavior is the basis for determining the variations in stresses during buckling. Classical buckling theory, by which is implied a membrane prebuckled shape, is used for the simply supported edge boundary conditions $\delta N_x = \delta v = \delta w = \delta M_x = 0$. Consequently, under all combinations of biaxial loading, the stress state is determinate. By use of knowledge of the stress state including its sign, i.e., whether it is tension or compression, the appropriate material properties are assigned. Next, a buckling criterion, derived herein, is applied to determine the buckling load under arbitrary combinations of axial and lateral pressure, including axial tension and external pressure as well as axial compression and internal pressure. A specific numerical example is treated to aid in understanding the type of results that are obtained. The results are then generalized in a form that reduces to Batdorf's classical k-Z form.[9]

Derivation of Buckling Criterion

The various moduli in the stress-strain relations for materials with different moduli in tension and compression are chosen in the Ambartsumyan model[5] according to the sign of the stresses in the (determinate) membrane prebuckled state.§ The stress-strain relations are then used to obtain the variations of the biaxial stresses during buckling. Subsequently, the variations of biaxial stresses are integrated through the shell thickness in order to obtain expressions for the variations of forces and moments during buckling. Finally, the variations of forces and moments are substituted in Donnell-type stability differential equations that are solved for simply supported edge boundary conditions. The result is a closed-form buckling criterion in terms of the material properties and geometry of the shell. The buckling criterion is applicable for arbitrary combinations of axial and lateral pressure, including one component of pressure that causes tension.

Stress-Strain Relations for Materials with Different Moduli in Tension and Compression

Ambartsumyan and Khachatryan[6] display stress-strain relations for a material with different elastic moduli in tension and compression. If the material is subjected to pure tension, the modulus is E_t in any direction (see Fig. 1). Similarly, under pure compression, the modulus is E_c in any direction. Poisson's ratios ν_t and ν_c characterize the lateral compression under uniaxial tension and the lateral expansion under uniaxial compression, respectively. For biaxial stress states of mixed tension and compression, the moduli are then E_t and E_c, respectively, and the Poisson's ratios are ν_t and ν_c, respectively. The strain-stress relations in principal stress coordinates are

$$\epsilon_x = a_{11}\sigma_x + a_{12}\sigma_y \tag{1a}$$

$$\epsilon_y = a_{12}\sigma_x + a_{22}\sigma_y \tag{1b}$$

where the a_{ij} are related to the elastic moduli and Poisson's ratios as follows:

$$\text{if } \sigma_x > 0 \text{ and } \sigma_y > 0, \text{ then } a_{11} = 1/E_t \tag{2a}$$

$$a_{12} = -\nu_t/E_t,\ a_{22} = 1/E_t$$

$$\text{if } \sigma_x < 0 \text{ and } \sigma_y < 0, \text{ then } a_{11} = 1/E_c \tag{2b}$$

$$a_{12} = -\nu_c/E_c,\ a_{22} = 1/E_c$$

$$\text{if } \sigma_x > 0 \text{ and } \sigma_y < 0, \text{ then } a_{11} = 1/E_t \tag{2c}$$

$$a_{12} = -\nu_t/E_t = -\nu_c/E_c,\ a_{22} = 1/E_c$$

$$\text{if } \sigma_x < 0 \text{ and } \sigma_y > 0, \text{ then } a_{11} = 1/E_c \tag{2d}$$

$$a_{12} = -\nu_c/E_c = -\nu_t/E_t,\ a_{22} = 1/E_t$$

Ambartsumyan and Khachatryan[6] prove that Eq. (2) satisfies the reciprocal relations

$$\nu_c E_t = \nu_t E_c \tag{3}$$

They also show that, in the nonprincipal stress coordinates α and β,

$$\gamma_{\alpha\beta} = \tau_{\alpha\beta}/G_{tc} \tag{4}$$

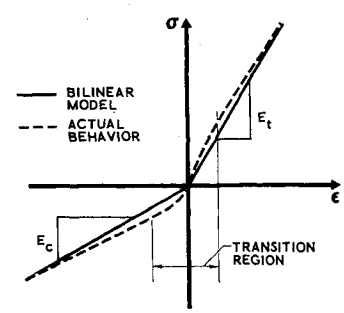

Fig. 2 Comparison of actual stress-strain behavior with the bilinear model.

‡ The reader is cautioned that the Russian word *soprotivlenie* is often incorrectly translated in the context of the present topic as *strength* rather than its proper meaning *stiffness* or *resistance*. This situation is quite unfortunate for those individuals who must carefully select key words in literature searches in order to avoid being overwhelmed by information, i.e., they are very likely to miss papers on the present topic.

§ Others might choose the moduli according to the sign of the strain or some weighted stress or strain intensity. However, the Ambartsumyan model is apparently the only workable model at present. Validation of an appropriate material model awaits definitive biaxial experimentation directed toward materials with different resistance in tension and compression.

where

$$G_{tc} = 1\Big/\left\{2\left[(a_{11} - a_{12})\frac{\sigma_x}{\sigma_x - \sigma_y} - (a_{22} - a_{12})\frac{\sigma_y}{\sigma_x - \sigma_y}\right]\right\} \tag{5}$$

is the shear modulus and depends only on the principal stresses. That is G_{tc} is a constant in all coordinates. However, in principal coordinates, $\tau_{\alpha\beta} = 0$ so the value of G_{tc} is immaterial then except, as will be seen, for the purpose of defining variations of the stresses σ_x, σ_y, and τ_{xy}. If $\sigma_x = \sigma_y$, then $a_{11} = a_{22}$ and the expression in Eq. (5) reduces to

$$G_{tc} = 1/[2(a_{11} - a_{12})] \tag{6}$$

The stress-strain relations in principal coordinates are obtained by inversion of Eq. (1):

$$\sigma_x = [1/(a_{11}a_{22} - a_{12}^2)](a_{11}\epsilon_x - a_{12}\epsilon_y) \tag{7a}$$

$$\sigma_y = [1/(a_{11}a_{22} - a_{12}^2)](-a_{12}\epsilon_x + a_{22}\epsilon_y) \tag{7b}$$

Variations of Stresses and Strains during Buckling

During buckling, the stresses vary from their prebuckling values in the manner shown in Fig. 4. There, the variations of stresses take place according to the sign of the pertinent stress and the corresponding modulus. Let the variation be denoted by δ. Then, from Eq. (7) and the inverse of Eq. (4),

$$\delta\sigma_x = K_{11}\delta\epsilon_x + K_{12}\delta\epsilon_y \tag{8a}$$

$$\delta\sigma_y = K_{12}\delta\epsilon_x + K_{22}\delta\epsilon_y \tag{8b}$$

$$\delta\tau_{xy} = K_{33}\delta\gamma_{xy} \tag{8c}$$

where

$$K_{11} = a_{22}/(a_{11}a_{22} - a_{12}^2) \qquad K_{12} = -a_{12}/(a_{11}a_{22} - a_{12}^2) \tag{9a}$$

$$K_{22} = a_{11}/(a_{11}a_{22} - a_{12}^2) \qquad K_{33} = G_{tc} \tag{9b}$$

The K_{ij} in Eq. (8) are analogous to the orthotropic functions K_{ij}^k in Eq. (2) of Jones.[10] In the case of materials with equal moduli in tension and compression, the K_{ij} reduce to

$$K_{11} = K_{22} = E/(1 - \nu^2), \quad K_{12} = \nu E/(1 - \nu^2), \quad K_{33} = E/[2(1 + \nu)] \tag{10}$$

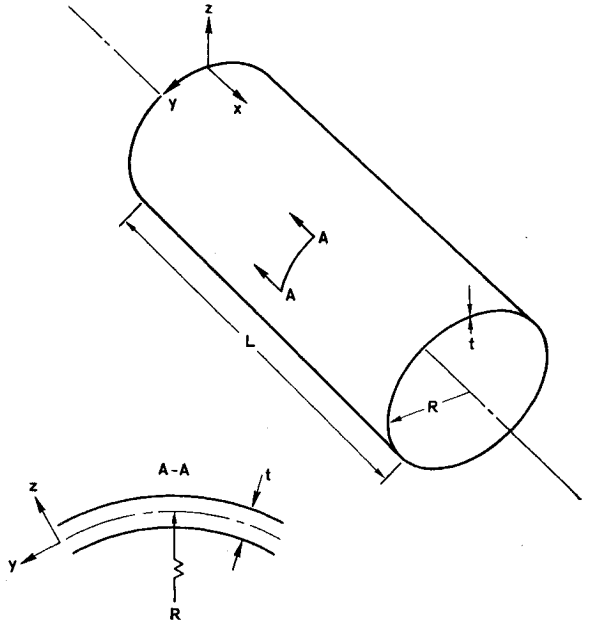

Fig. 3 Circular cylindrical shell.

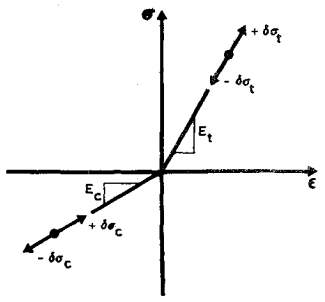

Fig. 4 Variations of stresses for a material with different moduli in tension and compression.

In Eq. (8), $\delta\epsilon_x$, $\delta\epsilon_y$, and $\delta\gamma_{xy}$ denote the variations in the strains during buckling and, because of the Kirchhoff-Love hypothesis, are

$$\delta\epsilon_x = \delta\epsilon_1 + z\delta\chi_1, \quad \delta\epsilon_y = \delta\epsilon_2 + z\delta\chi_2, \quad \delta\gamma_{xy} = \delta\epsilon_3 + z\delta\chi_3 \tag{11}$$

where z is the distance from the shell middle surface (see Fig. 3). In Eq. (11), $\delta\epsilon_1$, $\delta\epsilon_2$, and $\delta\epsilon_3$ are the variations of the middle surface strains

$$\delta\epsilon_1 = \delta u_{,x} \quad \delta\epsilon_2 = \delta v_{,y} + \delta w/R \quad \delta\epsilon_3 = \delta u_{,y} + \delta v_{,x} \tag{12}$$

and $\delta\chi_1$, $\delta\chi_2$, and $\delta\chi_3$ are the variations of the middle surface curvatures

$$\delta\chi_1 = -\delta w_{,xx} \quad \delta\chi_2 = -\delta w_{,yy} \quad \delta\chi_3 = -2\delta w_{,xy} \tag{13}$$

Upon substitution of the variations of strains, Eq. (11), in the variations of stresses, Eq. (8),

$$\delta\sigma_x = K_{11}(\delta\epsilon_1 + z\delta\chi_1) + K_{12}(\delta\epsilon_2 + z\delta\chi_2) \tag{14a}$$

$$\delta\sigma_y = K_{12}(\delta\epsilon_1 + z\delta\chi_1) + K_{22}(\delta\epsilon_2 + z\delta\chi_2) \tag{14b}$$

$$\delta\tau_{xy} = K_{33}(\delta\epsilon_3 + z\delta\chi_3) \tag{14c}$$

Variations of Forces and Moments during Buckling

The variations of forces and moments during buckling are obtained by integration of the variations of stresses through the shell thickness,

$$\delta N_x = \int_{-t/2}^{t/2} \delta\sigma_x dz \tag{15a}$$

$$\delta M_x = \int_{-t/2}^{t/2} \delta\sigma_x z dz \tag{15b}$$

The integrations yield

$$\delta N_x = B_{11}\delta\epsilon_1 + B_{12}\delta\epsilon_2 \tag{16a}$$

$$\delta N_y = B_{12}\delta\epsilon_1 + B_{22}\delta\epsilon_2 \tag{16b}$$

$$\delta N_{xy} = B_{33}\delta\epsilon_3 \tag{16c}$$

$$\delta M_x = D_{11}\delta\chi_1 + D_{12}\delta\chi_2 \tag{17a}$$

$$\delta M_y = D_{12}\delta\chi_1 + D_{22}\delta\chi_2 \tag{17b}$$

$$\delta M_{xy} = D_{33}\delta\chi_3 \tag{17c}$$

where

$$B_{ij} = K_{ij}t \tag{18}$$

$$D_{ij} = K_{ij}t^3/12 \tag{19}$$

For materials with equal moduli in tension and compression, the extensional and bending stiffnesses in Eqs. (18) and (19) reduce to the usual definitions upon substitution of the K_{ij} in Eq. (10), i.e.,

$$B_{11} = B_{22} = B = Et/(1 - \nu^2) \tag{20a}$$

$$B_{12} = \nu B \tag{20b}$$

$$B_{33} = [(1 - \nu)/2]B = Et/[2(1 + \nu)] \tag{20c}$$

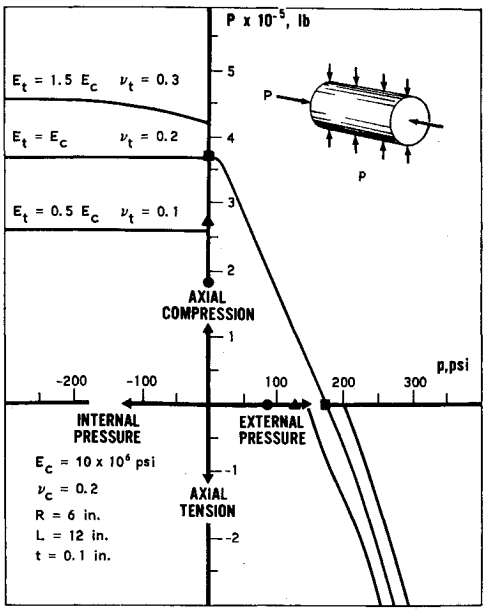

Fig. 5 Biaxial buckling behavior of a circular cylindrical shell with various tensile moduli.

$$D_{11} = D_{22} = D = Et^3/[12(1 - \nu^2)] \quad (20d)$$

$$D_{12} = \nu D \quad (20e)$$

$$D_{33} = [(1 - \nu)/2]D = Et^3/[24(1 + \nu)] \quad (20f)$$

Stability Differential Equations

The Donnell-type stability differential equations for circular cylindrical shells subjected to combinations of axial compression and lateral pressure are[11]

$$\delta N_{x,x} + \delta N_{xy,y} = 0 \quad (21a)$$

$$\delta N_{xy,x} + \delta N_{y,y} = 0 \quad (21b)$$

$$-\delta M_{x,xx} + 2\delta M_{xy,xy} - \delta M_{y,yy} + \delta N_y/R + \bar{N}_x\delta w_{,xx} + \bar{N}_y\delta w_{,yy} = 0 \quad (21c)$$

Upon substitution of the expressions for the variations of forces and moments during buckling [Eqs. (16) and (17)] and the variations of middle surface strains and curvatures [Eqs. (12) and (13)], the stability differential equations, Eq. (21), become

$$B_{11}\delta u_{,xx} + B_{12}(\delta v_{,xy} + \delta w_{,x}/R) + B_{33}(\delta u_{,yy} + \delta v_{,xy}) = 0 \quad (22a)$$

$$B_{12}\delta u_{,xy} + B_{22}(\delta v_{,yy} + \delta w_{,y}/R) + B_{33}(\delta u_{,xy} + \delta v_{,xx}) = 0 \quad (22b)$$

$$(B_{12}/R)\delta u_{,x} + (B_{22}/R)(\delta v_{,y} + \delta w/R) + D_{11}\delta w_{,xxxx} + 2(2D_{33} + D_{12})\delta w_{,xxyy} + D_{22}\delta w_{,yyyy} + \bar{N}_x\delta w_{,xx} + \bar{N}_y\delta w_{,yy} = 0 \quad (22c)$$

Buckling Criterion

It is desired to find the solution to the stability differential equations for the simply supported edge boundary conditions

$$\delta N_x = \delta v = \delta w = \delta M_x = 0 \quad (23)$$

The following buckling displacements satisfy the boundary conditions of Eq. (23):

$$\delta u = \bar{u}\cos(m\pi x/L)\cos(ny/R) \quad (24a)$$

$$\delta v = \bar{v}\sin(m\pi x/L)\sin(ny/R) \quad (24b)$$

$$\delta w = \bar{w}\sin(m\pi x/L)\cos(ny/R) \quad (24c)$$

and are substituted in the stability differential equations, Eq. (22), to yield homogeneous equations in $\bar{u}$, $\bar{v}$, and $\bar{w}$. In order for a nontrivial solution to exist to the homogeneous equations, i.e., an exact solution to the stability differential equations, the determinant of the coefficients of $\bar{u}$, $\bar{v}$, and $\bar{w}$ must be zero, and the following buckling criterion results:

$$\bar{N}_x(m\pi/L)^2 + \bar{N}_y(n/R)^2 = A_{33} + A_{23}[(A_{13}A_{12} - A_{11}A_{23})/(A_{11}A_{22} - A_{12}^2)] + A_{13}[(A_{12}A_{23} - A_{13}A_{22})/(A_{11}A_{22} - A_{12}^2)] \quad (25)$$

where

$$A_{11} = B_{11}(m\pi/L)^2 + B_{33}(n/R)^2 \quad (26a)$$

$$A_{12} = (B_{12} + B_{33})(m\pi/L)(n/R) \quad (26b)$$

$$A_{13} = (B_{12}/R)(m\pi/L) \quad (26c)$$

$$A_{22} = B_{33}(m\pi/L)^2 + B_{22}(n/R)^2 \quad (26d)$$

$$A_{23} = (B_{22}/R)(n/R) \quad (26e)$$

$$A_{33} = D_{11}(m\pi/L)^4 + 2(2D_{33} + D_{12})(m\pi/L)^2(n/R)^2 + D_{22}(n/R)^4 + B_{22}/R^2 \quad (26f)$$

The solution represented by Eq. (25) reduces to that of Block, Card, and Mikulas[12] for unstiffened single-layered shells with equal moduli in tension and compression. The buckling load calculated from Eq. (25) depends on the geometry, material properties, and buckling mode parameters m and n. To find the minimum buckling load for a specified range of discrete values of m and n, the minimization procedure described by Jones[13] is used. Because of the numerous repetitive calculations in the minimization procedure, the many variables in Eq. (25), and the need to determine the material moduli from the membrane prebuckled state, a computer program[14] is essential to the practical calculation of buckling loads.

The applied in-plane forces, $\bar{N}_x$ and $\bar{N}_y$, can be related to a positive number λ in the manner

$$\bar{N}_x = k_1\lambda, \quad \bar{N}_y = k_2\lambda \quad (27)$$

where k_1 and/or k_2 can be negative, although buckling occurs only when one of k_1 or k_2 is positive. Then, the left-hand side of Eq. (25) can be written as

$$\bar{N}_x(m\pi/L)^2 + \bar{N}_y(n/R)^2 = \lambda[k_1(m\pi/L)^2 + k_2(n/R)^2] \quad (28)$$

The special cases of axial compression, lateral pressure, and hydrostatic pressure are obtained with $k_1 = 1$, $k_2 = 0$; $k_1 = 0$, $k_2 = 1$; and $k_1 = \frac{1}{2}$, $k_2 = 1$, respectively. More general cases of biaxial loading are obtained by specifying other values of k_1 and k_2, including cases wherein one of k_1 or k_2 is negative.

Numerical Example

Before generalization of the buckling criterion, it is appropriate to consider a particular numerical example so that certain behavior characteristics can be understood without the penalty of the generalization parameters. The example involves a circular cylindrical shell of 6-in. radius, 12-in. length, and 0.1-in. thickness with a compressive modulus E_c of 10×10^6 psi, a compressive Poisson's ratio ν_c of 0.2, and the following tensile moduli and Poisson's ratios: $E_t = 5 \times 10^6$ psi and $\nu_t = 0.1$; $E_t = 10 \times 10^6$ psi and $\nu_t = 0.2$; and $E_t = 15 \times 10^6$ psi and $\nu_t = 0.3$. Note that in each case the reciprocal relations, $\nu_c E_t = \nu_t E_c$ [Eq. (2)], are satisfied.

The buckling loads for the aforementioned shell are shown in Fig. 5. The behavior of the shell in the axial compression-external pressure quadrant is the same irrespective of the tensile modulus. There, tension is not excited due to the

membrane prebuckling state stipulation. There is, of course, no buckling in the axial tension-internal pressure quadrant for circular cylindrical shells.

The most striking observation that can be made about Fig. 5 is that for $E_t < E_c$ there is a sharp drop in buckling load on passing from the axial compression-external pressure quadrant to either the axial tension-external pressure quadrant or the axial compression-internal pressure quadrant. Conversely, a sharp rise occurs for $E_t > E_c$. These discontinuities arise in Fig. 5 because the compliances a_{ij} in the stress-strain relations, Eq. (1), change in a discontinuous fashion upon passing from a biaxial compression state to a stress state involving both tension and compression. These discontinuities in compliances occur because of the slope discontinuity in the Ambartsumyan stress-strain model shown schematically in Fig. 1. Then, note in Fig. 4 that, at an unstressed point (the origin), the variation in stress can have two different signs and two different moduli. Such an unstressed point occurs, for example, in the axial direction in a shell loaded by external pressure or in the circumferential direction in a shell loaded by axial compression. Thus, only as the slightest amount of tension is applied does the shell "know" it has (significantly) different moduli in tension and compression. The resulting step change in the compliances causes a large change in buckling load essentially at a point. That is, the Ambartsumyan material model implies that the shell is either more or less stiff and, hence, either more or less buckling resistant in one direction or another depending on the loading.

The tensile modulus apparently plays an important role in buckling in the tension-compression quadrants of loading, but none at all in the biaxial compression quadrant. This fact should not be particularly surprising for a biaxial configuration such as a shell. Indeed, for a uniaxial configuration such as a ring, the circumferential bending stiffness D_{22} provides the primary buckling resistance and, of course, involves the compressive modulus. However, for buckling of long circular cylindrical shells under external pressure, the lowest buckling load is approximately

$$p_{cr} = (5.51/LR^{3/2})(1 - \nu_t\nu_c)^{1/4}D_{22}^{3/4}B_{11}^{1/4} \qquad (29)$$

Equation (29) is obtained from Eq. (25) by letting (n/R) $(m\pi/L)$ dominate for $m = 1$ and minimizing the resulting expression (an equivalent form is derived in the next section). Thus, the dominant terms are D_{22}, which involves the compressive modulus, and B_{11}, which involves the tensile modulus if only the slightest amount of axial tension occurs.

The sharp drop or rise in buckling load around pure external pressure or pure axial compression would be eliminated if the Ambartsumyan model and its inherent slope discontinuity were replaced by a continuous stress-strain curve as indicated by the dashed line in Fig. 2. However, the only portion of the present results that would be affected occurs around the discontinuities. The remainder of the present results are valid and would be approached by the more accurate material model after the discontinuities were smoothed out.

Two other behavior features are observed in Fig. 5. First, the presence of internal pressure does not increase the net axial compression buckling load when $E_t \leq E_c$ (the net load is the axial load less the internal pressure component in the axial direction). The reason for this characteristic is that axisymmetric buckling ($n = 0$) predominates, so lateral pressure does not appear in Eq. (25). For $E_t = 1.5E_c$, asymmetric buckling ($n \neq 0$) occurs as internal pressure increases until, at about 300 psi, axisymmetric buckling occurs and the curve becomes flat. The second behavior characteristic is related to the shape of the $E_t = 0.5E_c$ curve in the external pressure-axial tension quadrant. There, the addition of axial tension initially has little effect, but the "slope" of the effect rapidly becomes large and then decreases to more or less parallel the other curves as more axial tension is added. This type of behavior is more apparent in Figs. 9b and 9c.

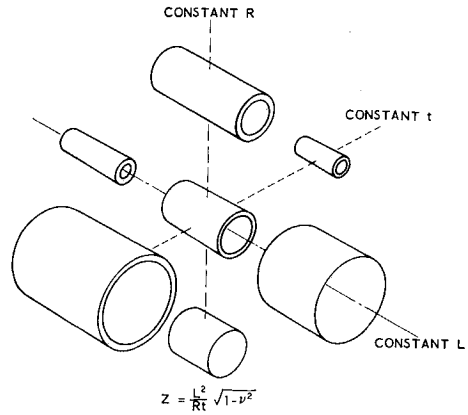

Fig. 6 Representative circular cylindrical shells corresponding to the same value of Z (Z about 150) (after Batdorf).

Because of the aforementioned discontinuities in pure axial compression loading and pure external pressure loading, the fact that some composite materials have a lower tensile modulus than compressive modulus is particularly important. The buckling behavior is very sensitive to the value of the tensile modulus even though a predominantly compressive load may act. This sensitivity is especially acute when the possibility exists of a small axial tension acting when predominantly external pressure is the supposed design condition (or a small internal pressure acts in conjunction with an apparently predominate axial compression). A reduction in the external buckling pressure from 175 to 146 psi, or 17%, occurs for the present shell if the tensile modulus is half the compressive modulus. A 30% reduction in axial buckling load occurs for the same shell.

Some of the possible approximate methods of treating shells with different moduli in tension and compression are illustrated with the use of Fig. 5. The particular case of shells with tensile moduli that are half the compressive moduli is discussed first. The exact solution is denoted by the line labeled $E_t = 0.5E_c$; its intersections with the axial compression axis and the external pressure axis will be compared with approximate results. Three possible modulus approximations for a single modulus theory are 1) lowest modulus (denoted by a dot at 1.8×10^5 lb on the axial compression axis and at 85 psi on the external pressure axis); 2) compression modulus (denoted by a square at 3.7×10^5 lb and 175 psi, respectively); and 3) average modulus (denoted by a triangle at 2.7×10^5 lb and 130 psi, respectively). Obviously, the lowest modulus (in this case the tensile modulus) corresponds to a grossly conservative buckling prediction because it is too low by 30% for axial compression and by 42% for external pressure. Use of the compression modulus alone leads to unconservative results, i.e., the buckling predictions are too high by 43% for axial compression and by 20% for external pressure. Use of the average modulus yields results that are unconservative by only 4% for axial compression, but for external pressure the average modulus results are conservative by 11%. Similar results could be shown for $E_t = 1.5E_c$ in Fig. 5. Thus, the merit of using the present approach to treating shells with different moduli in tension and compression is established.

Generalization of Buckling Criterion

For single-layered circular cylindrical shells with a single Young's modulus in tension and compression, the governing

stability differential equation and solution can be written[9] so that Batdorf's loading parameter k and curvature parameter Z are characteristic parameters. The physical significance of the Batdorf curvature parameter, $Z = (L^2/Rt)(1 - \nu^2)^{1/2}$, is displayed in Fig. 6. There, a single value of Z is seen to represent many different shell geometries. For that single value of Z, there corresponds a single loading parameter k which, in turn, determines the appropriate buckling load.

The objective of this section is to display a similar manner of general representation of results for buckling of circular cylindrical shells with different moduli in tension and compression under various combinations of axial and lateral pressure. The first step is to write the buckling criterion Eq. (25) in the form

$$\bar{N}_x(m\pi/L)^2 + \bar{N}_y(n/R)^2 = D_{11}(m\pi/L)^4 + 2(2D_{33} + D_{12})(m\pi/L)^2(n/R)^2 + D_{22}(n/R)^4 + B_{11}B_{22}B_{33}(1 - \nu_t\nu_c)(m\pi/L)^4(1/R^2)/[B_{11}B_{33}(m\pi/L)^4 + (B_{11}B_{22} - B_{12}^2 - 2B_{12}B_{33}) \times (m\pi/L)^2(n/R)^2 + B_{22}B_{33}(n/R)^4] \quad (30)$$

Buckling under Axial Compression

For axial compression, $\bar{N}_y = 0, a_{11} = 1/E_c$, and $a_{22} = 1/E_t$ so Eq. (30) can be rearranged to read

$$k_x = m^2\left[1 + 2\frac{1 + \nu_t}{1 + \nu_c}\left(\frac{nL}{m\pi R}\right)^2 + \frac{E_t}{E_c}\left(\frac{nL}{m\pi R}\right)^4\right] + \frac{12Z_{tc}^2}{m^2\pi^4}\Bigg/\left[1 + 2\frac{E_t}{E_c}\left(\frac{nL}{m\pi R}\right)^2 + \frac{E_t}{E_c}\left(\frac{nL}{m\pi R}\right)^4\right] \quad (31)$$

in which

$$k_x = \bar{N}_xL^2/\pi^2D_{11} = PL^2/2\pi^3RD_{11} \quad (32)$$

and

$$Z_{tc} = (L^2/Rt)[(E_t/E_c)(1 - \nu_t\nu_c)]^{1/2} \quad (33)$$

Note that the tensile modulus is used in the direction perpendicular to that of the principal load. Note also that Z_{tc} reduces to Batdorf's Z when $E_t = E_c$ and $\nu_t = \nu_c$ and has the same geometric interpretation as in Fig. 6.

For short shells, $Z_{tc} = 0$ so Eq. (31) reduces to

$$k_x = m^2\left\{1 + 2\frac{1 + \nu_t}{1 + \nu_c}\left(\frac{nL}{m\pi R}\right)^2 + \frac{E_t}{E_c}\left(\frac{nL}{m\pi R}\right)^4\right\} \quad (34)$$

This expression for $k_x(m,nL/m\pi R)$ achieves a stationary value when

$$\partial k_x/\partial m = 0 \quad (35)$$

$$\frac{\partial k_x}{\partial(nL/m\pi R)} = 0 \quad (36)$$

Note that m and $nL/m\pi R$ are treated as independent variables by virtue of Eqs. (35) and (36) despite the appearance of m in $nL/m\pi R$. However, $nL/m\pi R$ is to be regarded as a ratio of axial buckle wavelength to circumferential buckle wavelength, so it actually is an independent variable. Alternatively, $nL/m\pi R$ can be regarded as another form of n when m is fixed. This same distinction is made throughout the present section. From application of Eq. (36), it is seen that n must be zero, whereupon it is obvious that $m = 1$ provides a minimum to k_x (m cannot be zero if buckling is to occur) or

$$k_x = 1 \quad (37)$$

irrespective of the modulus ratio E_t/E_c. Equation (37) is the correct result for buckling of a long flat plate compressed in the short direction and simply supported along the long edges.[9] Recall that k_x depends on the bending stiffness D_{11} which, in turn, depends on the modulus ratio. Thus, although the normalized buckling load does not depend on the modulus ratio, the actual buckling load P does.

For long shells, the possibility exists of either axisymmetric or asymmetric buckling. Consider first axisymmetric buckling ($n = 0$) for which Eq. (31) becomes

$$k_x = m^2 + 12Z_{tc}^2/m^2\pi^4 \quad (38)$$

A stationary value of $k_x(m^2)$ occurs when

$$dk_x/d(m^2) = 1 - 12Z_{tc}^2/m^4\pi^4 = 0 \quad (39)$$

from which

$$m^4 = 12Z_{tc}^2/\pi^4 \quad (40)$$

The corresponding stationary value of k_x can be shown to be a minimum by verifying that $d^2k_x/d(m^2)^2 > 0$. Thus,

$$k_x = [4(3)^{1/2}/\pi^2]Z_{tc} = 0.702Z_{tc} \quad (41)$$

which looks like the usual equal-modulus long shell result[9] with the exception that, since Z_{tc} depends on the modulus ratio, E_t/E_c, so does k_x. However, Eq. (41) does enable the ready calculation of buckling loads via simple calculation involving Z_{tc}.

For asymmetric buckling of long shells, determination of the lowest buckling load involves finding a stationary value of k_x relative to m and $nL/m\pi R$, i.e., Eqs. (35) and (36). Upon substitution of the result of performing the operation indicated in Eq. (35) on Eq. (31) in the result of Eq. (36), the value of m^2 is found to be

$$m^2 = \frac{Z_{tc}}{\pi^2}\left\{3\Big/\left[1 + \left(\frac{E_t}{E_c}\right)^{1/2}\right]\left[1 + \frac{1 + \nu_t}{1 + \nu_c}\left(\frac{E_c}{E_t}\right)^{1/2}\right]\right\}^{1/2} \quad (42)$$

That this value of m^2 provides a minimum to the value of k_x can be shown by investigation of the sign of the second derivatives of k_x with respect to m^2 and $(nL/m\pi R)^2$. The minimum normalized buckling load is

$$k_x = \frac{4(3)^{1/2}}{\pi^2}Z_{tc}\left\{\left[1 + \frac{1 + \nu_t}{1 + \nu_c}\left(\frac{E_c}{E_t}\right)^{1/2}\right]\Big/\left[1 + \left(\frac{E_t}{E_c}\right)^{1/2}\right]\right\}^{1/2} \quad (43)$$

Whether this asymmetric buckling load is lower than the axisymmetric buckling load from Eq. (41) depends obviously on the value of the bracketed quantity in Eq. (43). If $E_t/E_c > 1$, the bracketed quantity is less than 1 and, then, the asymmetric buckling load is less than the axisymmetric buckling load. If $E_t/E_c < 1$, the bracketed quantity is greater than 1 and, then, the axisymmetric buckling load is less than the asymmetric buckling load. For $E_t/E_c = 1$ (the isotropic equal-modulus case), the bracketed quantity is 1, so the asymmetric and axisymmetric buckling loads are identical.

The minimization procedure formulated by Jones[13] is used in the author's computer program[14] to determine the lowest k_x in Eq. (31) for admissible (integer) values of m and n. Shells are not considered which are of such proportions and material properties that buckling is governed by the Euler column result. The lowest k_x is plotted in Fig. 7 as a function of Z_{tc} for $E_t = kE_c$ where $k \leq 1$ and for $E_t = 2E_c$. Note that the numerical results from the computer program properly tend toward the short shell value, $k_x = 1$ from Eq. (37), as Z_{tc} goes to zero. Also note that, for long shells, the axisymmetric buckling behavior predicted by use of Eq. (41) for $E_t = kE_c$ where $k \leq 1$ is achieved as is the asymmetric buckling behavior of Eq. (43) for $E_t = 2E_c$. The smooth curve connecting the short and long shell regions represents the lower bound of all numerical results. That is, the curve

is obtained by connecting the bottoms of cusps in the curves for particular R/t ratios.

In Fig. 7, results that correspond to a particular geometry (i.e., a particular L^2/Rt) but different moduli in Eq. (33) are shown as dots. Note that, for $E_t = kE_c$ where $k \leq 1$, i.e., for axisymmetric buckling, changing the modulus ratio merely changes Z_{tc} along a single curve. On the other hand, for $E_t > E_c$, i.e., asymmetric buckling, changing the modulus ratio defines a new $k_x - Z_{tc}$ curve.

Buckling under Lateral Pressure

For lateral (external) pressure, $\bar{N}_x = 0$, $a_{11} = 1/E_t$, and $a_{22} = 1/E_c$, so Eq. (30) can be written as

$$k_y = m^2\left[\frac{E_t}{E_c}\left(\frac{m\pi R}{nL}\right)^2 + \frac{1+\nu_t}{1+\nu_c} + \left(\frac{nL}{m\pi R}\right)^2\right] + \frac{12Z_{tc}^2}{m^2\pi^4}\Bigg/ \left[\frac{E_t}{E_c}\left(\frac{nL}{m\pi R}\right)^2 + 2\frac{E_t}{E_c}\left(\frac{nL}{m\pi R}\right)^4 + \left(\frac{nL}{m\pi R}\right)^6\right] \quad (44)$$

in which

$$k_y = \frac{\bar{N}_y L^2}{\pi^2 D_{22}} = \frac{pRL^2}{\pi^2 D_{22}} \quad (45)$$

and Z_{tc} is defined in Eq. (33). As in the case of axial compression, the tensile modulus is used in the direction perpendicular to that of the principal loading.

For short shells, $Z_{tc} = 0$, so Eq. (44) becomes

$$k_y = m^2\left[\frac{E_t}{E_c}\left(\frac{m\pi R}{nL}\right)^2 + 2\frac{1+\nu_t}{1+\nu_c} + \left(\frac{nL}{m\pi R}\right)^2\right] \quad (46)$$

A stationary value of $k_y(nL/m\pi R)$ occurs when

$$dk_y/d(nL/m\pi R) = 0 \quad (47)$$

which results in

$$(nL/m\pi R)^2 = (E_t/E_c)^{1/2} \quad (48)$$

Equation (48) provides a minimum to $k_y(nL/m\pi R)$ since it can be shown that

$$d^2k_y/d(nL/m\pi R)^2 > 0 \quad (49)$$

Upon substitution of Eq. (48) in Eq. (46) and recognition that a minimum of k_y $(m^2,nL/m\pi R)$ occurs for $m = 1$, the lowest normalized buckling load is found to be

$$k_y = 2[(E_t/E_c)^{1/2} + (1+\nu_t)/(1+\nu_c)] \quad (50)$$

For the equal-modulus case, Eq. (50) correctly reduces to the value $k_y = 4$, the buckling load of a long flat plate compressed in the long direction and simply supported along the long edges.[9]

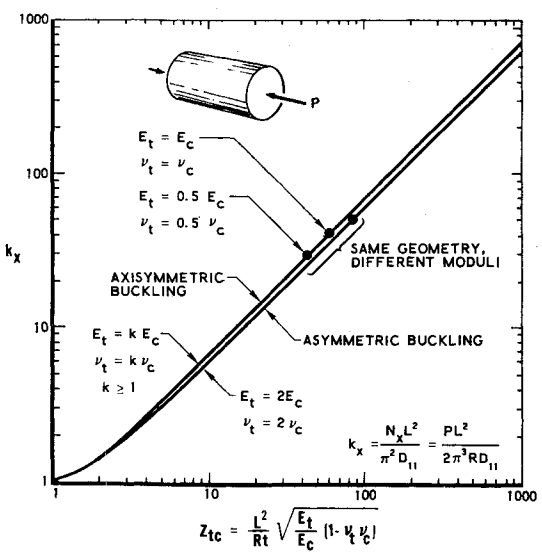

Fig. 7 Axial compression buckling results.

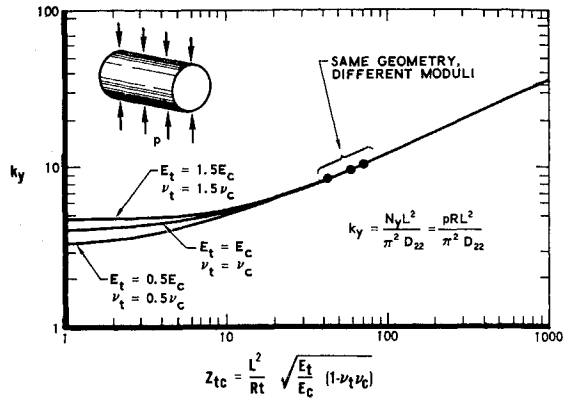

Fig. 8 Lateral pressure buckling results.

For long shells, the factor $(nL/m\pi R)$ is much greater than 1, so Eq. (44) becomes

$$k_y = m^2\left(\frac{nL}{m\pi R}\right)^2 + \frac{12Z_{tc}^2}{m^2\pi^4}\Bigg/\left(\frac{nL}{m\pi R}\right)^6 \quad (51)$$

A stationary value to $k_y(nL/m\pi R)$ occurs when

$$\frac{dk_y}{d(nL/m\pi R)} = 2m^2\left(\frac{nL}{m\pi R}\right) - \frac{72Z_{tc}^2}{m^2\pi^4}\Bigg/\left(\frac{nL}{m\pi R}\right)^7 = 0 \quad (52)$$

from which it is seen that

$$(nL/m\pi R)^8 = 36Z_{tc}^2/m^4\pi^4 \quad (53)$$

Substitution of Eq. (53) in Eq. (51) yields

$$k_y = m\frac{4(6)^{1/2}}{3\pi}Z_{tc}^{1/2} \quad (54)$$

The lowest normalized buckling load occurs at $m = 1$:

$$k_y = [4(6)^{1/2}/3\pi]Z_{tc}^{1/2} = 1.04Z_{tc}^{1/2} \quad (55)$$

which looks like the usual equal-modulus long shell result.[9] However, since Z_{tc} depends on the modulus ratio E_t/E_c, so does k_y. Thus, the value of Z_{tc} alone determines k_y. That is, for long shells, lateral pressure buckling behavior is governed by a single straight line irrespective of E_t/E_c. From examination of Eq. (33), it is apparent that changing E_t/E_c can be thought of as changing the effective length of the shell. In particular, it is seen from Eq. (55) that increasing E_t/E_c increases the buckling pressure as is expected.

As in the case of axial compression, the author's computer program[14] is used to determine the lowest k_y in Eq. (44) for admissible (integer) values of m and n. The lowest k_y is plotted in Fig. 8 as a function of Z_{tc} for three values of E_t/E_c ($E_t = 0.5E_c, E_c$, and $1.5E_c$) with corresponding ν_t and ν_c. Shells long enough and with R/t such that the $n = 2$ mode governs are not considered. Thus, the present results represent an extension of a simplified version of Batdorf's results (Fig. 1 of Ref. 9). The numerical results in Fig. 8 for short shells properly approach the flat plate results given by Eq. (50). For long shells, the results in Fig. 8 agree with Eq. (55). The various k_y and corresponding Z_{tc} obtained for shells of identical geometry but with three different E_t/E_c are shown as dots in Fig. 8.

Buckling under Biaxial Loading

Interest in buckling of shells under biaxial loading has increased in recent years because of increasingly complex structural loads. General k-Z results are derived and presented in this section for the following biaxial loading combinations:

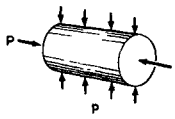

LOADING PARAMETERS	MATERIAL PROPERTIES		
$k_x = \frac{\bar{N}_x L^2}{\pi^2 D_{11}} = \frac{PL^2}{2\pi^3 RD_{11}}$	CURVE	E_t	ν_t
	1	$0.5E_c$	$0.5\nu_c$
$k_y = \frac{\bar{N}_y L^2}{\pi^2 D_{22}} = \frac{prL^2}{\pi^2 D_{22}}$	2	E_c	ν_c
	3	$1.5E_c$	$1.5\nu_c$

Fig. 9a Definition of parameters for biaxial results.

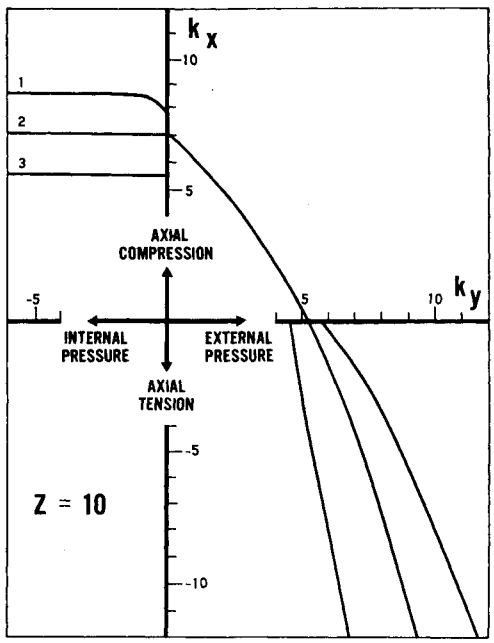

Fig. 9b Biaxial buckling results for $Z = 10$.

1) axial compression-internal pressure and 2) lateral (external) pressure-axial tension in addition to the more common case of 3) axial compression-lateral (external) pressure. The biaxial tension quadrant is ignored because circular cylindrical shells do not buckle under that loading.

For axial compression and internal pressure, Eq. (30) can be written as

$$k_x = \tilde{k}_x/[1 + k_2(nL/m\pi R)^2] \tag{56}$$

where $\tilde{k}_x$ is defined as the right-hand side of Eq. (31), k_2 is the proportion of circumferential load defined in Eq. (27), and k_x is defined in Eq. (32). The right-hand side of Eq. (56) could be minimized with respect to discrete mode numbers m and n by the procedure due to Jones[13] to obtain the value of k_x at buckling. However, Eq. (56) is used merely to demonstrate the existence of a k_x and a Z_{tc} for biaxial loading. The actual determination of $\bar{N}_x$ and $\bar{N}_y$ from Eq. (25) is made in the author's computer program.[14] Subsequently, k_x and k_y are calculated from Eqs. (32) and (45).

For lateral (external) pressure and axial tension, Eq. (30) can be written as

$$k_y = \tilde{k}_y/[1 + k_1(m\pi R/nL)^2] \tag{57}$$

where $\tilde{k}_y$ is defined as the right-hand side of Eq. (44), k_1 is the proportion of axial loading defined in Eq. (27), and k_y is defined in Eq. (45). The values of k_x and k_y are determined as described in the preceding paragraph.

In both Eqs. (56) and (57), Z_{tc} is a characteristic parameter. Thus, general results can be presented for all k_1 and k_2 when

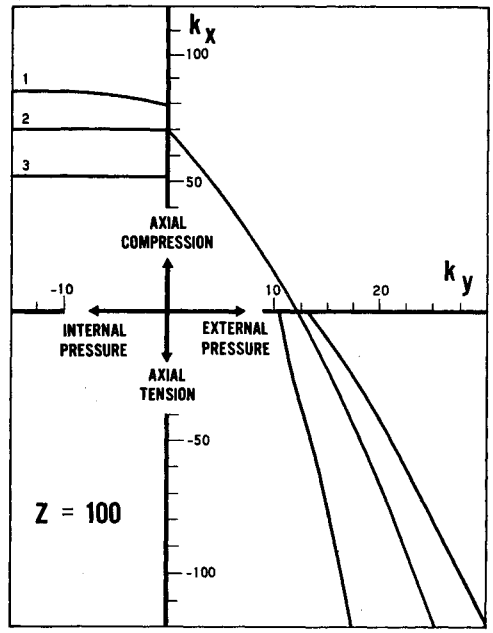

Fig. 9c Biaxial buckling results for $Z = 100$.

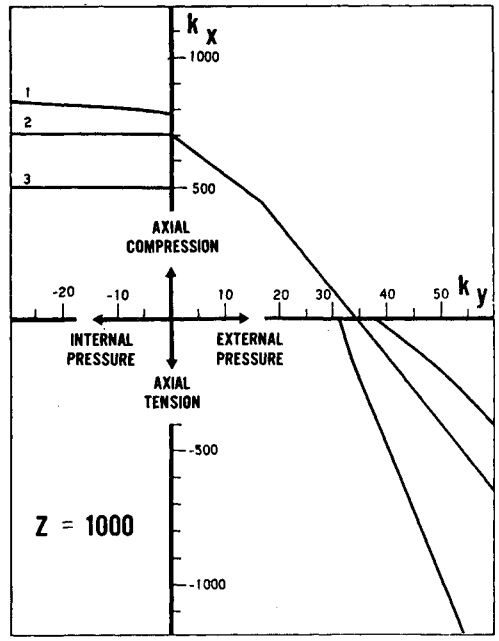

Fig. 9d Biaxial buckling results for $Z = 1000$.

a specific modulus ratio, E_t/E_c, is chosen for a specific Z_{tc}. Alternatively, general results can be presented for a specific geometry (L^2/Rt in Z_{tc}) for various E_t/E_c. The latter approach is taken in Fig. 9. There, the geometry is that of Z_{tc} for $E_t = E_c = E$ (and, hence, $\nu_t = \nu_c = \nu$), or Z, by definition. Basic definitions of loading parameters and material properties are displayed in Fig. 9a. Results are presented for $Z = 10$, 100, and 1000 in Figs. 9b, c, and d, respectively, for E_t equal to $0.5E_c$,E_c, and $1.5E_c$.

The representative general results in Fig. 9 exhibit all the features already described for the simpler problem in the Numerical Example Section. Note that, as Z increases from 10 to 100 to 1000 in Figs. 9b, c, and d, respectively, k_x increases faster than k_y. This behavior can be predicted by superposition of Figs. 7 and 8 (see Fig. 5 of Ref. 9).

The general results in Figs. 7–9 give a representative basis on which to assess the buckling behavior of circular cylindri-

cal shells with different elastic moduli in tension and compression. Results for other modulus ratios can be obtained crudely by interpolation or extrapolation on Figs. 7–9, or more accurately by use of the author's computer program.[14]

Concluding Remarks

An exact solution for buckling of circular cylindrical shells with different elastic moduli in tension and compression is derived for arbitrary combinations of axial and lateral pressure. The combinations include those in which one component of pressure causes tension. The material model is due to Ambartsumyan[5] and involves a bilinear stress-strain curve that has a discontinuity in slope (modulus) at the origin. Classical buckling theory, by which is implied a membrane prebuckled shape, is used for a set of simply supported edge boundary conditions.

General biaxial buckling results in a form analogous to Batdorf's classical k-Z form[9] are presented for several ratios of tensile to compressive moduli. Differences in the tensile and compressive moduli are observed to cause significant differences in the buckling loads. (These differences are mainly a consequence of the discontinuities in the material model.) This situation is particularly acute when only a small tensile loading component exists in conjunction with an apparently dominant compressive loading component. For example, if a small axial loading is present in a principally external pressure loading environment, a reduction of 17% in the external pressure buckling load from the zero axial load case occurs for a tensile modulus that is half the compressive modulus.

The present results are important because current composite materials often have significantly different elastic moduli in tension and compression. However, to the author's knowledge, definitive biaxial buckling experiments have not been performed on shells made of composite materials exhibiting such behavior. Thus, the present theoretical results cannot be compared with experiments, but serve as a strong impetus for the generation of high quality experimental data.

References

[1] Ambartsumyan, S. A., "Specific Peculiarities of a Theory of Shells from Modern Materials," *Izvestiya Akademii Nauk Armianskoi SSR, Mekhanika*, Vol. 21, No. 4, 1968, pp. 3–19; translation available from STAR as N69-27721.

[2] Davis, J. W. and Zurkowski, N. R., *Put the Strength and Stiffness Where You Need It*, Rept. T-STDB(101.05)R, Reinforced Plastics Division, Minnesota Mining and Manufacturing Co., Minneapolis, Minn.

[3] Seldin, E. J., "Stress-Strain Properties of Polycrystalline Graphites in Tension and Compression at Room Temperature," *Carbon*, Vol. 4, 1966, pp. 177–191.

[4] Babel, H. W., private communication, McDonnell/Douglas Astronautics Co., Santa Monica, Calif., Feb. 1969.

[5] Ambartsumyan, S. A., "The Axisymmetric Problem of a Circular Cylindrical Shell Made of Material with Different Stiffness in Tension and Compression," *Izvestiya Akademii Nauk SSSR, Mekhanika*, No. 4, 1965, pp. 77–85; translation available from STAR as N69-11070.

[6] Ambartsumyan, S. A. and Khachatryan, A. A., "Basic Equations in the Theory of Elasticity for Materials with Different Stiffness in Tension and Compression," *Inzhenernyi Zhurnal, Mekhanika Tverdogo Tela*, No. 2, 1966, pp. 44–53; translation available as LRG-67-T-12, The Aerospace Corp., El Segundo, Calif.

[7] Ambartsumyan, S. A., "Equations of the Plane Problem of the Multimodulus Theory of Elasticity," *Izvestiya Akademii Nauk Armianskoi SSR, Mekhanika*, Vol. 19, No. 2, 1966, pp. 3–19; translation available as LRG-67-T-14, The Aerospace Corp., El Segundo, Calif.

[8] Ambartsumyan, S. A. and Khachatryan, A. A., "Theory of Multimodulus Elasticity," *Inzhenernyi Zhurnal, Mekhanika Tverdogo Tela*, No. 6, 1966, pp. 64–67; translation available from STAR as N67-27610.

[9] Batdorf, S. B., "A Simplified Method of Elastic-Stability Analysis for Thin Cylindrical Shells," Rept. 874, 1947, NACA.

[10] Jones, R. M., "Buckling of Circular Cylindrical Shells with Multiple Orthotropic Layers and Eccentric Stiffeners," *AIAA Journal*, Vol. 6, No. 12, Dec. 1968, pp. 2301–2305; also *Errata*, Vol. 7, No. 10, Oct. 1969, p. 2048.

[11] Donnell, L. H., "Stability of Thin-Walled Tubes under Torsion," Rept. 479, 1933, NACA.

[12] Block, D. L., Card, M. F., and Mikulas, M. M., Jr., "Buckling of Eccentrically Stiffened Orthotropic Cylinders," TN D-2960, Aug. 1965, NASA.

[13] Jones, R. M., "Plastic Buckling of Eccentrically Stiffened Multilayered Circular Cylindrical Shells," *AIAA Journal*, Vol. 8, No. 2, Feb. 1970, pp. 262–270.

[14] Jones, R. M., "Buckling of Circular Cylindrical Shells with Different Moduli in Tension and Compression," TR-0066(S5816-70)-2, Reissue A, June 1970, The Aerospace Corp., San Bernardino, Calif.; available only from CFSTI (Dept. of Commerce).